MNRAS 000, 1–5 (2015) Preprint 2 October 2020 Compiled using MNRAS LATEX style file v3.0

HD 110113 b (TOI-755.01)- a hot mini-Neptune transiting a Sun-like star

H.P. Osborn,[1,2]★, D.J. Armstrong[3,4], V. Adibekyan[5], E. Delgado-Mena[5], G. King[3,4], J.F. Otegi[6], N.C. Santos,[5,7]

[1]*NCCR/PlanetS, Centre for Space & Habitability, University of Bern, Bern, Switzerland*
[2]*Department of Physics and Kavli Institute for Astrophysics and Space Research, MIT, 70 Vassar Street, Cambridge, MA 02139, USA*
[3]*Centre for Exoplanets and Habitability, University of Warwick, Gibbet Hill Road, Coventry, CV4 7AL, UK*
[4]*Department of Physics, University of Warwick, Gibbet Hill Road, Coventry CV4 7AL, UK*
[5]*Instituto de Astrofísica e Ciências do Espaço, Universidade do Porto, CAUP, Rua das Estrelas, 4150-762 Porto, Portugal*
[6]*Geneva Observatory, University of Geneva, Chemin des Mailettes 51, 1290 Versoix, Switzerland*
[7]*Departamento de Física e Astronomia, Faculdade de Ciências, Universidade do Porto, Rua do Campo Alegre, 4169-007 Porto, Portugal*

Accepted XXX. Received YYY; in original form ZZZ

ABSTRACT

We report the discovery of HD 110113 b (TOI-755.01), a transiting mini-Neptune exoplanet on a 2.5-day orbit around a sunlike G-type star ($T_{\rm eff}$= 5730K). Using *TESS* photometry and HARPS radial velocities, we find HD 110113 b has a radius of 2.06 ± 0.14 $R_\oplus$ and a mass of 4.56 ± 0.6 $M_\oplus$. The resulting density of $2.85^{+0.76}_{-0.62}$ g cm^{-3} is significantly lower than would be expected from a pure-rock world, therefore HD 110113 b must be a mini-Neptune with significant volatile atmosphere. Given the high incidental flux and low surface-gravity of the planet, we find it unusual that HD 110113 b was able to hold onto it's atmosphere over its $\sim$ 4Gyr lifetime. We also find a non-transiting planet with a mass of 10.5 ± 1.2 $M_\oplus$and a period of $6.745^{+0.009}_{-0.008}$ d, although a strong stellar rotation signal with period $22.5^{+3.8}_{-1.6}$ d impedes its confirmation.

Key words: planets and satellites: detection – stars: individual: HD110113

1 INTRODUCTION

2 OBSERVATIONS

2.1 TESS photometry

HD 110113was observed during *TESS*sector 10 with 2-minute cadence for 22.5 days, excluding a 2.5 day gap between TESS orbits to downlink data. The lightcurve was processed using the Pre-Search Data Conditioning (PDC) pipeline, producing precise detrended photometry with typical precision of 150ppm/hr. This lightcurve was then searched for exoplanetary candidates with the SPOC (Science Processing Operations Centre). Vetting identified a strong candidate with a period of 2.54, a depth of only 400ppm and a Signal to Noise Ratio (SNR) of 7.6. It was designated TESS Object of Interest (TOI) 755.01.

2.2 HARPS RVs

Over the course of two observing seasons in 2018 and 2019, a total of N high-resolution spectra were taken with the High Accuracy Radial velocity Planet Searcher on the 3.4m telescope at La Silla, Chile. These radial velocities were taken as part of the NCORES program designed to specifically study the internal structure of hot worlds.

The HARPS spectra and derived RVs were accessed and downloaded through the DACE portal hosted at the University of Geneva (**?**).

2.3 Ground-based Photometric Observations

Karen ToDo

2.4 Speckle imaging

Howell ToDo

3 ANALYSIS

3.1 Stellar Parameters

Stellar parameters ($T_{\rm eff}$and $\log g$) and [Fe/H] were derived using a recent version of the MOOG code (Sneden 1973) and a set of plane-paralel ATLAS9 model atmospheres (Kurucz 1993). The analysis was done in LTE. The methodology used is described in detail in

★ E-mail: hugh.osborn@space.unibe.ch

Sousa et al. (2011) and Santos et al. (2013). The full spectroscopic analysis is based on the Equivalent Widths (EWs) of 233 Fe i and 34 Fe ii weak lines by imposing ionization and excitation equilibrium. The line-list used was taken from Sousa et al. (2008).

3.2 Combined RV and Photometric modelling

3.2.1 Treatment of Radial Velocities

All RV indicator statistics showed clear signs of stellar variability, likely due to the presence of starspots. To remove this stellar activity we first turned to linear decorrelation of the RV signal using RV indicators. The FWHM and S-index showed the clearest rotational signals, so selected these and used the decorrelation technique provided with the DACE radvel python package (**?**). Despite the activity indicators removing much of the stellar variability signal, the peak at $22.5^{+3.8}_{-1.6}$ remained strong in the radial velocity timeseries. After removing the rotation signal at $22.5^{+3.8}_{-1.6}$ by fitting a Keplerian, the next strongest signals were at $2.541^{+0.0}_{-0.001}$ d and $6.745^{+0.009}_{-0.008}$ d, followed by signals on longer periods which are most likely spurious due to rotational and observational aliases.

Instead of performing linear decorrelation, which clearly was not capable of adequately removing stellar rotation, we applied the same Gaussian process model to S-index, FWHM, and radial velocity simultaneously. The GP kernel used is a so-called "rotational" kernel built from the combination of two SHO kernels in `celerite`. Amplitude and mean function of each GP would differ All parameters were given broad priors, although the rotation period was constrained to the value obtained from a Lomb-Scargle periodogram with a standard deviation of 40%.

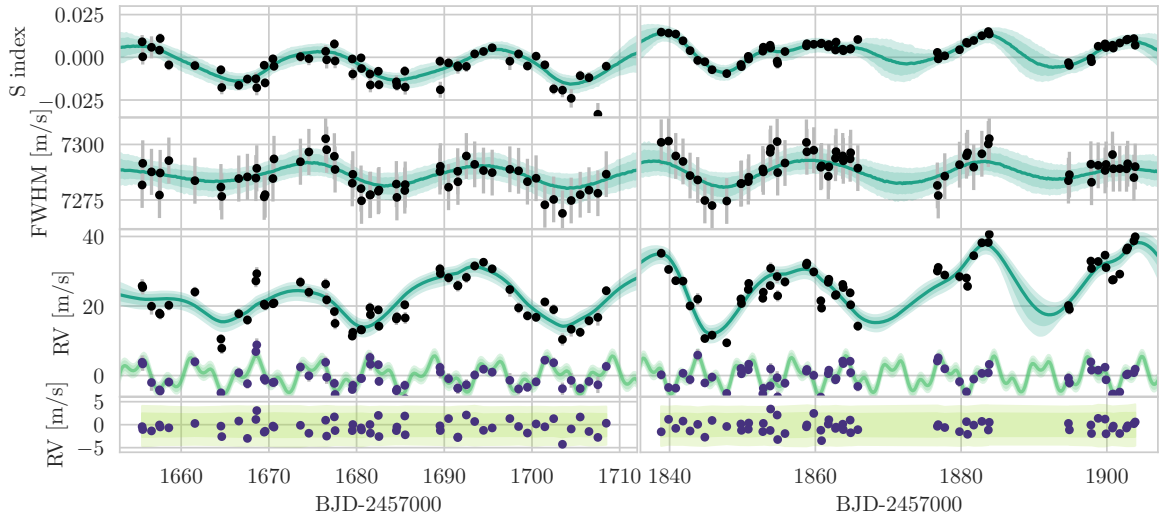

Figure 1. S-index, FWHM and RV timeseries, with GP models and 2-sigma uncertainty regions overplotted in green. Below the raw RV timeseries is the GP-removed timeseries showing the sum of the two planets models, and their uncertainties. At the very bottom the full model residuals are shown, with an RMS of only 1.50m/s, only 14cm/s above the average HARPS measurement uncertainties.

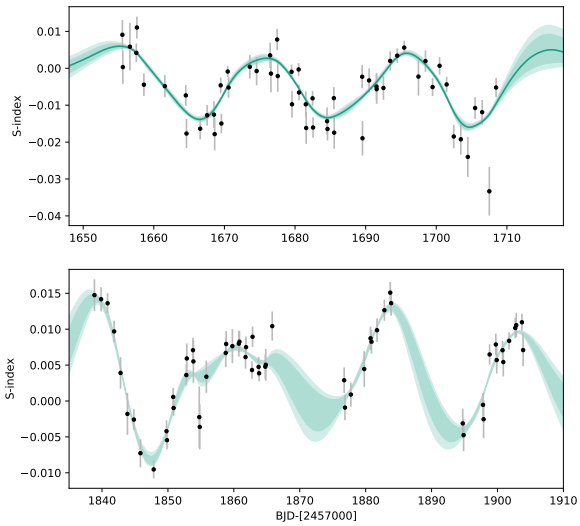

Figure 2. A timeseries of HARPS S-index, along with the best-fit Gaussian process model

We used PyMC3's "Interpolated" prior function to build specific prior functions for timescale, period, factor and mixing parameters such that their prior probability matched the posterior probabilities from the S-index those from the output of the S-index-trained model. We initially tried to use the same kernel hyperparameters to predict both RV and photometric time series deviations, this proved to not be possible, likely because the effect of stellar variability on photometry is not necessarily at the same timescale as for RVs (**?**). Instead we used a separate, single-SHO kernel with $Q = 1/\sqrt{2}$ to model the photometric stellar variability. This was also trained on a dataset without a planetary signal, as above for RVs, but in this case the out-of-transit photometry was used.

We modelled the log amplitude of both the RV (logK) and transit (logRp/Rs) signals to guard against negative masses or radii. Eccentricity was taken from the Kipping prior (), quadratic limb darkening parameters were reparameterised according to the `exoplanet` implementation of Kipping et al, and ror & b were similarly reparameterised following the `exoplanet` implementation of Espinoza et al. The compiled model was then optimised and sampled with `PyMC`'s NUTS sampler built into `exoplanet`, producing 2400 independent samples.

The results from the combined model are shown in figure 2 and table **??**.

As a cross-reference, these models were

3.2.2 *Treatment of photometry*

In the case of TESS data, although a Lomb-Scargle periodogram of the raw TESS lightcurve also shows peak variability with a period around 25d, the processed PDC lightcurve is flat, likely as variability on the order of a TESS orbit ($\sim 14d$) are removed during processing.

Table 1. This is an example table. Captions appear above each table. Remember to define the quantities, symbols and units used.

A	B	C	D
1	2	3	4
2	4	6	8
3	5	7	9

3.3 Other potential planet candidates

Both Kepler and TESS have shown that multi-planet systems of small planets in resonant orbits close to their star are common (**?**). Therefore, it is worth exploring whether signals of other candidate planets are present in either the TESS photometry or the RV time series.

We ran the `transit least squares` algorithm (**?**) on the model-subtracted lightcurve and found...

Present in the RV periodogram (and, interestingly, not in the activity periodograms) is a relatively strong peak at around 7 days. The best-fitting combined two-planet model (limiting planet c to non-transiting solutions) produces an outer planet with a potential mass of TBD on a period of TBD. The parameters for the planet b remain within errorbars Although `exoplanet` does not allow the computation of Bayesian evidence, we can use the log likelihoods of the best-fitting 1-planet model with the best-fitting 2-planet model to compute the difference in Bayesian Inference Criterium (ΔBIC. This value is TBD in favour of a TBD. However, such a peak also corresponds to exactly $P_{\rm rot}/3$, and may be an alias of the rotation period.

The corresponding `TLS` periodogram shows no peak at this period suggesting that, if it is due to an outer planet, the planet is either grazing or non-transiting. Such a candidate planet would likely also be near an $8/3$ resonance with HD 110113 b, and therefore could be characterised using TTVs. However, the low-SNR nature of this planet means that no significant TTVs are currently detectable. HD 110113 bwill be re-observed by *TESS*during Sector 37[1]

4 METHODS, OBSERVATIONS, SIMULATIONS ETC.

Normally the next section describes the techniques the authors used. It is frequently split into subsections, such as Section **??** below.

4.1 Discussion

5 CONCLUSIONS

The last numbered section should briefly summarise what has been done, and describe the final conclusions which the authors draw from their work.

[1] https://heasarc.gsfc.nasa.gov/cgi-bin/tess/webtess/wtv.py?Entry=73228647

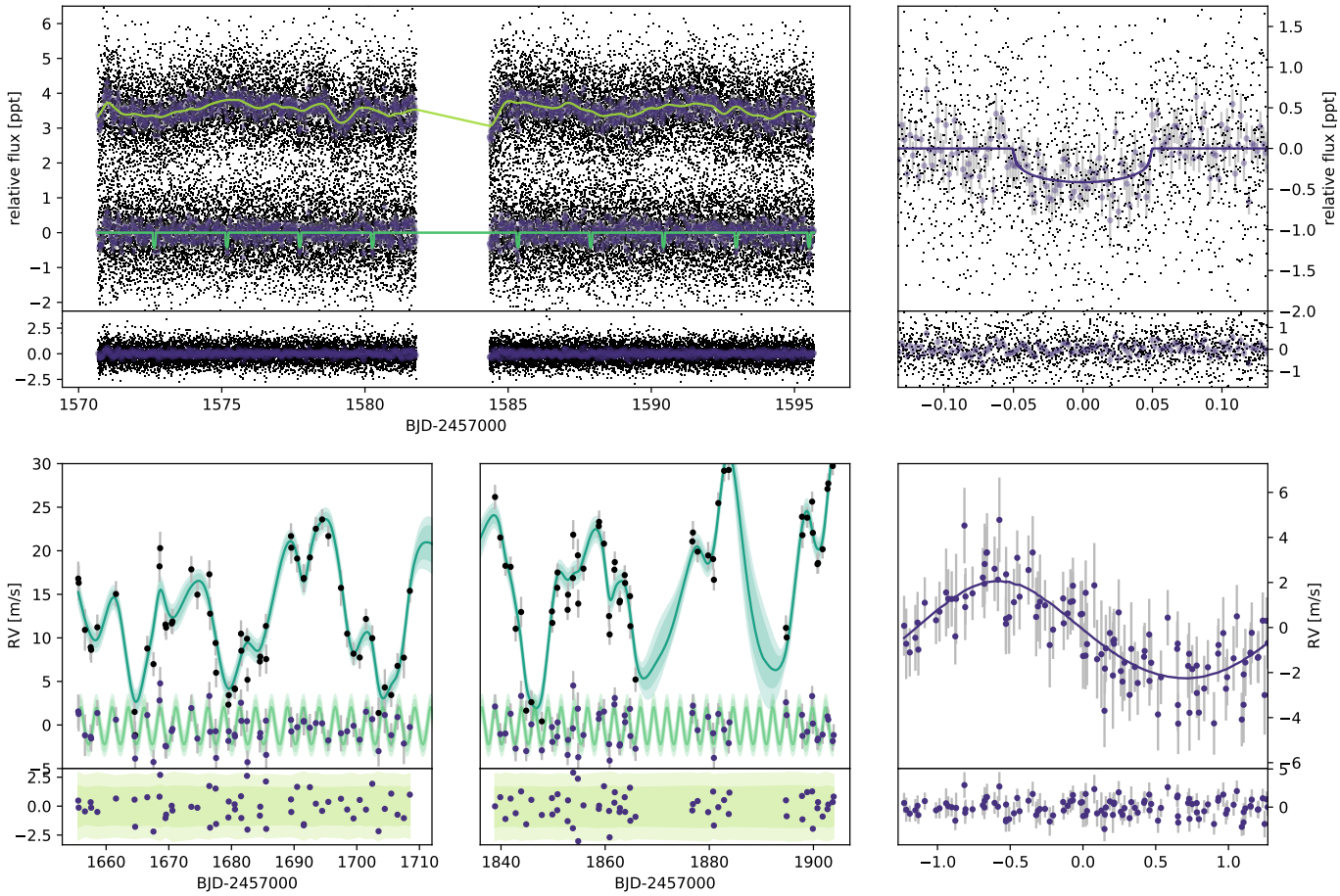

Figure 3. Photometric & RV time series. Detrended *TESS*Lightcurve both with and without best-fit Gaussian Process; transit model lightcurve residuals after subtraction of GP and transit model (centre left); Phase-folded lightcurve centred on transit with best-fit model (upper right); Phase-folded model residuals (centre right); Detrended HARPSRVs both with and without S-index-trained Gaussian Process model (lower left); RV residual time series after subtraction of GP and planet model (bottom left); Phase-folded RVs with best-fit RV model (lower right); Phase-folded RV residuals (bottom right).

ACKNOWLEDGEMENTS

APPENDIX A: SOME EXTRA MATERIAL

If you want to present additional material which would interrupt the flow of the main paper, it can be placed in an Appendix which appears after the list of references.

This paper has been typeset from a TEX/LATEX file prepared by the author.

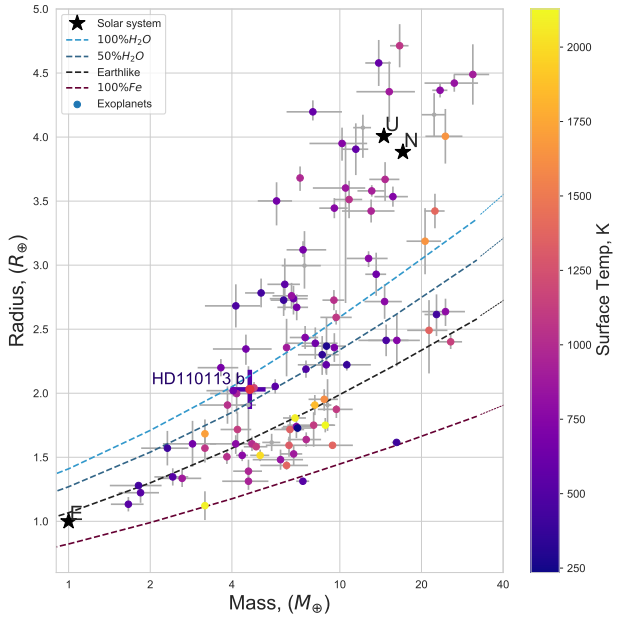

Figure 4. A Mass-Radius diagram for small planets with masses and radii constrained to better than SNR=4, with data from the NASA exoplanet archive (**?**). Colour coding shows the surface temperature of each planet (assuming an albedo of 0.2). Solar System planets are marked with stars.